UC San Diego
UC San Diego Previously Published Works

Title

Urea-based hydrothermal synthesis of LiNi0.5Co0.2Mn0.3O2 cathode material for Li-ion battery

Permalink

https://escholarship.org/uc/item/4hw4v1f8

Authors

Shi, Yang
Zhang, Minghao
Fang, Chengcheng
<u>et al.</u>

Publication Date

2018-08-01

DOI

10.1016/j.jpowsour.2018.05.030

Peer reviewed

Urea-based hydrothermal synthesis of $LiNi_{0.5}Co_{0.2}Mn_{0.3}O_2$ cathode material for Li-ion battery

Yang Shi, Minghao Zhang, Chengcheng Fang, Ying Shirley Meng*

Department of NanoEngineering, University of California San Diego, La Jolla, CA 92093-0448, USA

HIGHLIGHTS

- $LiNi_{0.5}Co_{0.2}Mn_{0.3}O_2$ cathode is synthesized by a urea-based hydrothermal method.
- The optimum synthesis is achieved with the precursor synthesized at 200 °C for 24 h.
- P-24 sample has better electrochemical performance than P-12 and P-18 samples.
- P-24 sample has high diffusivity and low charge transfer resistance.
- P-24 sample has low cation mixing and uniform distribution of transition metal.

ARTICLE INFO

ABSTRACT

A urea-based hydrothermal approach has been applied to synthesize $LiNi_{0.5}Co_{0.2}Mn_{0.3}O_2$ (NCM523) cathode materials with focus on investigating the influence of the reaction conditions on their electrochemical performance. The compositions of the carbonate precursor are precisely controlled by tuning urea concentration, hydrothermal reaction temperature, and time. The mole ratio between urea and transition metal ions and reaction temperature influence the composition of the precursor; while the reaction time influences the electrochemical performance of the final product. The optimized materials show better cyclability and rate capability compared with the materials synthesized with other hydrothermal reaction conditions. The enhancement is attributed to the larger Li^+ diffusion coefficient and lower charge transfer resistance, which are due to the lower degree of Li/Ni cation mixing and more uniform distribution of transition metal ions. This work is a systematic study on the synthesis of NCM523 cathode material by a urea-based hydrothermal approach.

1. Introduction

Lithium-ion battery is one of the most promising power source candidates for large-scale energy storage systems such as battery packs in smart grids and electric vehicles [1–3]. Layer-structured ternary materials $LiNi_{1-x-y}Co_xMn_yO_2$ have attracted much attention as cathode materials, in which $LiNi_{0.5}Co_{0.2}Mn_{0.3}O_2$ (NCM523) is viewed as a promising candidate due to its relatively high energy density and low cost [4,5]. Compared with $LiCoO_2$ cathode material, less use of Co reduces the cost; Ni contributes to a higher capacity at the expense of complicated preparation and Mn enhances the structural stability [6]. In the synthesis of these materials, the precursors play an important role on their electrochemical performances. The geometry, size, tap density and homogeneity of precursors well define these characteristics in the final products [7–10]. Therefore, various methods have been applied to synthesize NCM523 precursors, such as hydroxide co-precipitation

[11], carbonate co-precipitation [12], and sol-gel method [13]. However, a major drawback of hydroxide co-precipitation method is the oxidation of Mn^{2+} into Mn^{3+}, which results in manganese oxyhydroxide (MnOOH) impurity phases, and an inert atmosphere needs to be applied to prevent such oxidation [14]. Carbonate co-precipitation has the main advantage that the oxidation state of the cations is kept at 2 + for all transition metals in the carbonate matrix [15]. However, stirring speed and pH value need to be carefully monitored during the co-precipitation process [16]. The sol-gel method usually produces materials with low tap density and volumetric density, as well as it requires aging and time consuming drying steps [8].

A hydrothermal method is believed to improve the crystallinity of transition metal oxide materials, because the high vapor pressure decreases the activation energy for crystallization [17]. There are three kinds of hydrothermal-assisted approaches to synthesize cathode materials. The first kind of approach utilized the hydrothermal reaction

between high concentration lithium hydroxide (LiOH) solutions and hydroxide precursors synthesized by co-precipitation, including previous research on hydrothermal synthesis of NCM523 [18] and $LiNi_{1/3}Co_{1/3}Mn_{1/3}O_2$ (NCM111) [19–22] cathode materials. When NCM111 cathode material was synthesized through hydrothermal method for the first time, the hydrothermal treatment lasted 4 days at 170 °C [19]. NCM523 cathode material was also synthesized with similar approach, yet with a high temperature at 250 °C [18]. The second kind of approach is the synthesis of the final product through a one-step hydrothermal reaction by adding transition metal ions and LiOH aqueous solution together in the autoclave. However, high concentration of LiOH solution (4M) and excess amount of LiOH (Li: (Ni + Co + Mn) = 20:1) had to be used in such methods to guarantee the production of a pure layered phase [23]. This is not cost-effective considering the price of lithium salt and the cost of recycling and re-using LiOH solution. The third kind of approach is the synthesis of precursors through hydrothermal reactions. Ryu et al. used a solvo/hydrothermal method to synthesize $Ni_{1/3}Mn_{1/3}Co_{1/3}CO_3$ precursor, which was later sintered with lithium carbonate (Li_2CO_3) to form $LiNi_{1/3}Mn_{1/3}Co_{1/3}O_2$ [24]. The hydrothermal synthesis of precursors requires neither long treatment time and high temperature, nor the using of high concentration and excess amount of LiOH solution. Therefore, hydrothermal synthesis of precursors is utilized in this work to produce NCM523 cathode material.

Urea had been used as fuel and chelating agent in the synthesis of doped $LiCoO_2$ [25], $LiNi_{0.5}Mn_{1.5}O_4$ spinel [26–28], lithium-rich cathode materials [29], and CoNiAl three-component layered double hydroxides [30]. The decomposition of urea releases CO_3^{2-} slowly at elevated temperature, and the following reaction can happen [31], which allows the precursor to precipitate:

$$CO(NH_2)_2 + 2H_2O = 2NH_4^+ + CO_3^{2-} \qquad (1)$$
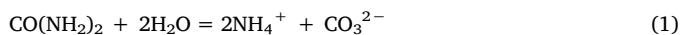
In this work, we used a urea-based hydrothermal method to synthesize a carbonate precursor $Ni_{0.5}Co_{0.2}Mn_{0.3}CO_3$, followed by sintering with Li_2CO_3. The parameters that influence the composition of the precursor are investigated and the electrochemical performances of NCM523 materials prepared with different precursors are tested. Energy-dispersive X-ray spectroscopy (EDS) and electrochemical impedance spectroscopy (EIS) were performed to investigate the reasons for the different electrochemical performances of synthesized NCM523 materials.

2. Experimental

Nickel acetate tetrahydrate ($Ni(Ac)_2 \cdot 4H_2O$, Aldrich, 99%), cobalt acetate tetrahydrate ($Co(Ac)_2 \cdot 4H_2O$, Sigma-Aldrich, 98%), manganese acetate tetrahydrate ($Mn(Ac)_2 \cdot 4H_2O$, Sigma-Aldrich, 99%), urea ($CO(NH_2)_2$, Sigma-Aldrich, 99%) and Li_2CO_3 (Sigma-Aldrich, 99%) were used as starting materials. The preparation of $Ni_{0.5}Co_{0.2}Mn_{0.3}CO_3$ precursor was as follows: $Ni(Ac)_2 \cdot 4H_2O$, $Co(Ac)_2 \cdot 4H_2O$, $Mn(Ac)_2 \cdot 4H_2O$ (Ni:Co:Mn = 5:2:3) and urea were dissolved in de-ionized water with different mole ratios of urea to transition metal cations, ranging from 2:1 to 3:1. The urea concentration was 0.25 M. After rigorous stirring for 30 min, the mixed solution was transferred into a Teflon-lined stainless steel autoclave and reacted at different temperatures ranging from 180 °C to 200 °C, and times ranging from 6 h to 24 h. The precipitated products were centrifuged at 6000 rpm, washed with de-ionized water for 5 times, and dried at 80 °C in the oven for 12 h. After the optimum urea-to-transition metal ratio and reaction temperature are figured out, three kinds of precursors with different reaction time of 12 h, 18 h, and 24 h at this optimum condition were utilized to produce NCM523 cathode materials, namely P-12, P-18, and P-24. The precursors and Li_2CO_3 were thoroughly mixed in the agate mortar, sintered at 500 °C for 5 h and at 900 °C for 12 h in air to obtain NCM523 powder.

The composition of the precursor and NCM523 powder was measured by an Inductively Coupled Plasma Optical Emission Spectrometer (ICP-OES, Perkin Elmer Optima 3000 DV). The morphology of NCM523 powder was observed by Scanning Electron Microscope (SEM, Phillips XL30). The tap density of the samples was measured by a powder tap density tester (JZ-1). The crystal structure of the powder was examined by X-ray Powder Diffraction (XRD) employing Cu K_α radiation by Rigaku MiniFlex XRD. The transition metal element distribution on the internal cross section of precursor and NCM523 powder were analyzed by EDS. More than 10 particles were examined for each sample to guarantee the repeatability of the measurement.

To prepare the samples for cross section view, the powder samples were added to polyvinylidene fluoride (PVDF) solution in 1-Methyl-2-pyrrolidinone (NMP). The dispersion was well mixed before being casted on microscope glass slide, followed by getting dried at 50 °C on a hotplate. The dried films were peeled off with a blade, immersed in liquid nitrogen for 30 s, bent and split into two pieces to expose the cross section of the powder.

To make electrodes, the synthesized NCM523 powder was mixed with PVDF, and carbon black (super P65) in NMP at a mass ratio of 8:1:1. Then the slurry was cast on Al foil using a doctor blade and dried in a vacuum oven at 80 °C for 24 h.

Disc electrodes were cut, compressed by a rolling mill and dried in a vacuum oven for 4 h before being transferred into an Ar-filled glovebox (H_2O < 0.5 ppm). The active mass loading was about 3 mg/cm^2 2016 coin cells were assembled with Li metal disc (thickness 1.1 mm) as anode, 1 M $LiPF_6$ in ethylene carbonate and ethyl methyl carbonate (EC: EMC 1:1 wt) as electrolyte, and trilayer membrane (Celgard 2320) as a separator.

The coin cells were rested for 2 h before the electrochemical tests were performed. Galvanostatic charge-discharge was carried out using an Arbin BT2000 battery testing system in the potential range of 3–4.3 V and 3–4.6 V at 20 mA g^{-1} for cycling stability test. The rate capability tests were performed at different current ranges from 20 mA g^{-1} to 400 mA g^{-1}. The electrochemical impedance spectroscopy (EIS) tests were carried out at the discharged state in the frequency range of 10^6 Hz to 10^{-2} Hz with signal amplitude of 5 mV by Solartron Impedance/Gain-Phase Analyzer after 50 cycles. The cathodes after 50 cycles were analyzed using X-ray photoelectron spectroscopy (XPS) (Kratos AXIS Supra) with Al Kα radiation. The spectra were calibrated by assigning the C 1s peak at 284.6 eV.

3. Results and discussion

To form $Ni_{0.5}Co_{0.2}Mn_{0.3}CO_3$ precipitation, the minimum mole ratio between urea and transition metal is 1:1 if all urea completely decomposes, which is not the case. Therefore, different mole ratios between urea and transition metals ranging from 2:1 and 3:1 are investigated with a reaction temperature of 200 °C. The composition of the corresponding precipitation products based on ICP measurement is displayed in Table 1. At 200 °C, when the mole ratio between urea and cations is 2:1 and 3:1, the concentration of Ni in the precursor is lower than expected, while an intermediate ratio of 5:2 delivers the target stoichiometry. The undesired chemical stoichiometry when the ratio is too low (2:1) or too high (3:1) comes from the competition between the carbonate co-precipitation reaction and the ammonia complex formation [15]. Ni^{2+} has higher solubility constant value ($K_{sp} = 1.4 \times 10^{-7}$) than Co^{2+} ($K_{sp} = 1 \times 10^{-10}$) and Mn^{2+} ($K_{sp} = 8.8 \times 10^{-11}$) and harder to precipitate [32]. Therefore, a sufficiently high CO_3^{2-} concentration is needed to guarantee a complete precipitation of Ni^{2+}, and a ratio of 2:1 is not high enough to provide sufficient CO_3^{2-}. On the other hand, the decomposition of urea releases NH_4^+, which could react with M^{2+} (M = Ni, Co and Mn) to produce soluble $[M(NH_3)_n]^{2+}$ in the solution [33]. Therefore a high concentration of urea (3:1 ratio) may lead to the formation of $[M(NH_3)_n]^{2+}$ complexes rather than carbonate precipitation. It is figured out that with an intermediate ratio

Table 1
Composition of carbonate precursors and residual transition metal concentration in solution under different synthesis conditions.

Temperature (°C)	n (urea): n (TM)	Time (h)	Precursor Ni:Co:Mn	Residual Ni^{2+} (mg/L)	Residual Co^{2+} (mg/L)	Residual Mn^{2+} (mg/L)
200	2:1	12	4.595:2:2.901	67.1	0.0063	0.0072
200	5:2	12	4.986:2:3.012	0.18	0.0021	0.0024
200	3:1	12	4.710:2:2.912	22.2	0.0035	0.0037
180	5:2	12	4.643:2:2.803	56.8	0.0044	0.0049
200	5:2	6	4.954:2:2.987	0.21	0.0017	0.0019
200	5:2	18	5.006:2:2.994	0.15	0.0012	0.0014
200	5:2	24	5.012:2:3.004	0.13	0.0009	0.0011

of 5:2, the desired stoichiometry of the precipitated product is attained. By keeping the same ratio of 5:2 and decreasing the reaction temperature to 180 °C, the precipitation of Ni^{2+} and Mn^{2+} is not complete, which indicates that a reaction temperature of 180 °C is not high enough. When the reaction time is extended to 18 h and 24 h, the composition of the precursor almost does not change, indicating that the cations have been fully precipitated.

Since the precipitated products can reach the target stoichiometry by using a reaction temperature of 200 °C and the urea-to-transition metal ratio of 5:2, the influence of reaction time at this condition is further investigated. When the reaction time is reduced to 6 h, Ni^{2+} cannot be completely precipitated. Therefore, three kinds of precursors with different reaction time of 12 h, 18 h, and 24 h were sintered with Li_2CO_3 to prepare the NCM523 material, namely P-12, P-18, and P-24. The ratios between Li, Ni, Co and Mn in P-12, P-18 and P-24 are confirmed by ICP-OES to be 10.02:4.99:2.01:3.01, 10.01:5.01:2.02:2.99 and 10.01:5.01:1.99:3.00, respectively. In the SEM images (Fig. 1), the secondary particles show a spherical morphology and each spherical secondary particle is made of primary grains with a diameter of 200–500 nm. With the extended time in hydrothermal synthesis of the precursor, there is no obvious change on the morphology of the particles. The tap densities of P-12, P-18, and P-24 samples are 2.54, 2.54 and 2.56 g/cm^3, respectively, which are comparable with those of the commercial samples CS-1 (TODA America NCM04ST, 2.63 g/cm^3) and CS-2 (MTI EQ-Lib-LNCM523, 2.60 g/cm^3).

The XRD patterns of these three types of powder are shown in a Fig. 2. A typical pattern of α-NaFeO$_2$ structure with $R\overline{3}$ m space group is observed, and the splits of the (006)/(102) and (108)/(110) peaks indicate the formation of layered structure [34]. XRD patterns are analyzed by Rietveld refinement and the results are displayed in Table 2. The atoms positions and occupancies are shown in Table S1. The a and c lattice parameters for each sample are similar. The higher value of intensity ratio $I_{(003)}/I_{(104)}$ indicates lower degree of Li/Ni cation mixing and better hexagonal layered structure [35]. The concentration of Ni^{2+}

on the Li^+ sites are 6.39%, 5.87% and 4.40% for P-12, P-18, and P-24 powder, respectively; P-24 has the lowest degree of cation mixing.

In the hydrothermal synthesis of precursors, urea gradually released CO_3^{2-} to precipitate the transition metal cations as temperature increases. Manganese is the easiest to be precipitated because the equilibrium constant of Manganese carbonate ($K_{sp} = 8.8 \times 10^{-11}$) is smaller than that of Cobalt carbonate ($K_{sp} = 1 \times 10^{-10}$), while Nickel is most difficult to be precipitated ($K_{sp} = 1.4 \times 10^{-7}$). Therefore, a concentration gradient might be formed in the precursors and the NCM powder. To determine the compositional change in the precursors and NCM powder, and investigate this effect on the electrochemical performance, EDS line scan is used to detect the composition on the cross-section of precursor and NCM powder, as displayed in Fig. 3. The concentrations of Ni, Co and Mn in precursors as a function of the distance are shown in Fig. 4 a–c. It is obvious that the Ni concentration increases gradually from the core to the surface of the particle, whereas the Mn concentration decreases gradually from the core to the surface; Co concentration remains relatively constant throughout the particle. The trend is consistent with the solubility constant values (K_{sp}) of the transition metal carbonate, i.e., the element which tends to precipitate first has higher value near the core and vice versa. Even though the absolute amount of the transition metal shows a trend of element distribution, it does not directly provide the information for a clear comparison between different types of precursor powder. Since EDS intensity values are dependent on the thickness of the site of interest, due to the geometry of the round particles, the core position would have higher intensities of transition metal than the position at the surface. Considering Co has a uniform distribution throughout the particle, it serves as a natural reference for comparison. Therefore, the intensity ratios of Ni/Co and Mn/Co are used to compare the Ni and Mn distributions and plotted as a function of distance (Fig. 4 d–f). It is clear that Ni and Mn distributions in the P-24 precursor are the most uniform, which means a longer time of hydrothermal treatment enables the diffusion and redistribution of Ni and Mn cations.
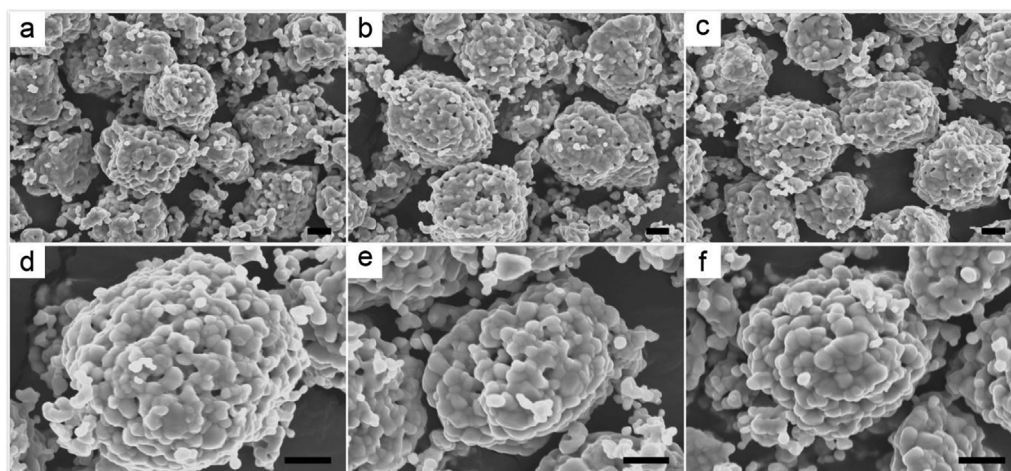

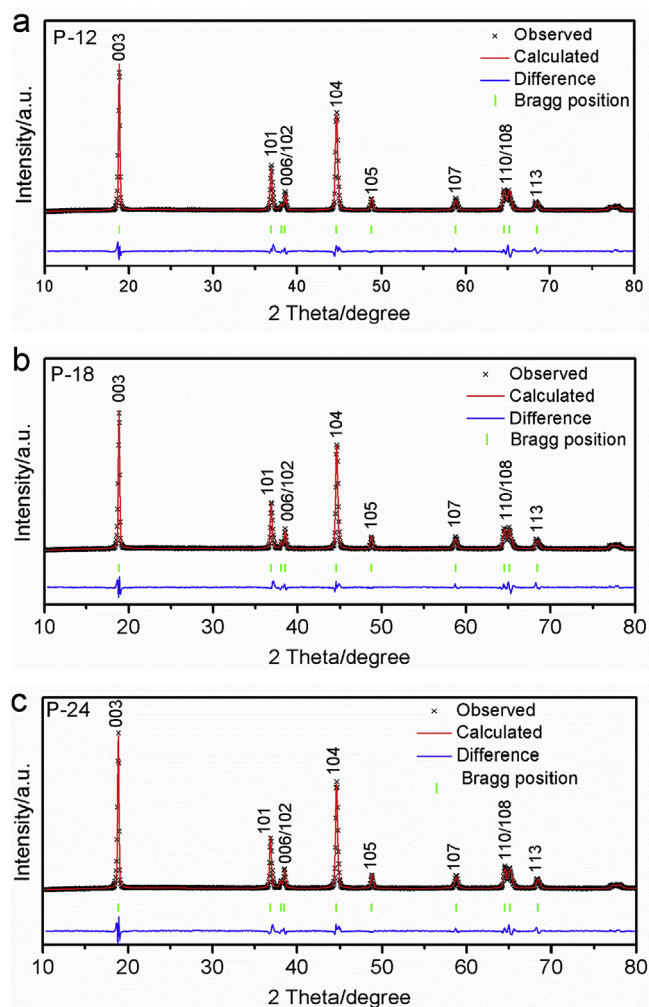**Fig. 1.** SEM images of NCM523 powder **(a, d)** P-12, **(b, e)** P-18, **(c, f)** P-24; the scale bar is 2 μm.

Fig. 2. XRD patterns of **(a)** P-12, **(b)** P-18 and **(c)** P-24 powder.

Table 2
Lattice parameters of NCM523 powder.

Samples	$a = b(Å)$	$c(Å)$	$I_{(003)}/I_{(104)}$	Ni in Li layer (%)	R_{wp} (%)	R_B (%)
P-12	2.868(0)	14.234(0)	1.311	6.39(2)	5.83	4.51
P-18	2.868(4)	14.239(3)	1.348	5.87(8)	5.89	4.29
P-24	2.868(2)	14.238(6)	1.459	4.40(8)	5.94	3.73

The transition metal intensities and intensity ratios of NCM powder sintered from the corresponding precursor are shown in Fig. 5. By comparing Fig. 4 a–c and Fig. 5 a–c, the NCM powder have more uniform distribution of transition metals, which means the transition metals diffuse and redistribute during the sintering process. This interdiffusion of transition metal ions is consistent with a previous report [10]. However, as shown in Fig. 5 d–f, P-24 powder still has more uniform distribution of Ni and Mn than P-12 and P-18. This indicates that the lithiation via high temperature sintering does not guarantee a uniformly distributed transition metal ions, which is also reported previously [36].

Fig. 6a shows the initial charge-discharge curves of NCM523 powder at $20\,mA\,g^{-1}$ between 3 and 4.3 V and their cycling performance. Three cells were assembled for each sample and the error bars show the variation from cell to cell. The initial discharge capacities are 145.3, 153.9, and 158.6 mAh g-1 for P-12, P-18 and P-24, respectively. P-24 has the highest initial capacity and the best cycling performance among the three. The capacity retention of P-12, P-18 and P-24 powder after 50 cycles is 89.5%, 91.0% and 92.6%, respectively. Their dQ/dV plots were obtained by differential analysis of the charge and discharge curves (Fig. 6b–d), and the redox peaks correspond to the plateaus in the charge and discharge curves. After cycling the oxidation peaks shift to higher voltage and the reduction peaks shift to lower voltage after cycles. P-24 sample has the smallest redox peaks shift while P-12 sample has the largest shift. This indicates that the P-24 sample has the smallest polarization among the three. As shown in Fig. 6e, the P-24 powder exhibits better rate capability than P-12 and P-18 powder. The voltage profiles are shown in Fig. 6e–g and the corresponding average voltage differences between charge and discharge cycles under different rates are displayed in Fig. 6i. P-24 cathode has the smallest difference between the average charge and discharge voltage, which further proves its smallest polarization. Since P-24 cathode has the best electrochemical performance among the three, which means a longer time of hydrothermal reaction in the synthesis of the precursor improves the overall performance. Therefore, the cathode material was also prepared with the precursor after a hydrothermal reaction of 30 h, namely P-30. Its cycling stability is only slightly better than the P-24 cathode (Supplementary Fig. S1). Considering a longer reaction is time-consuming and the electrochemical performance is barely improved, a hydrothermal reaction of 24 h is believed to be the optimum condition for the synthesis of precursors with this approach. Since cycling at a higher upper cut-off voltage is an effective way to evaluate the stability of the synthesized material, P-12, P-18 and P-24 samples were also cycled at $20\,mA\,g^{-1}$ in the voltage range of 3–4.6 V. As shown in Fig. 6j, the P-12, P-18, P-24 samples show discharge capacities of 190.8, 195.1, and $200.0\,mAh\,g^{-1}$ in the first cycle and capacity retention of 71.3%, 73.5%, and 79.4% after 50 cycles, respectively. With a higher cut-off
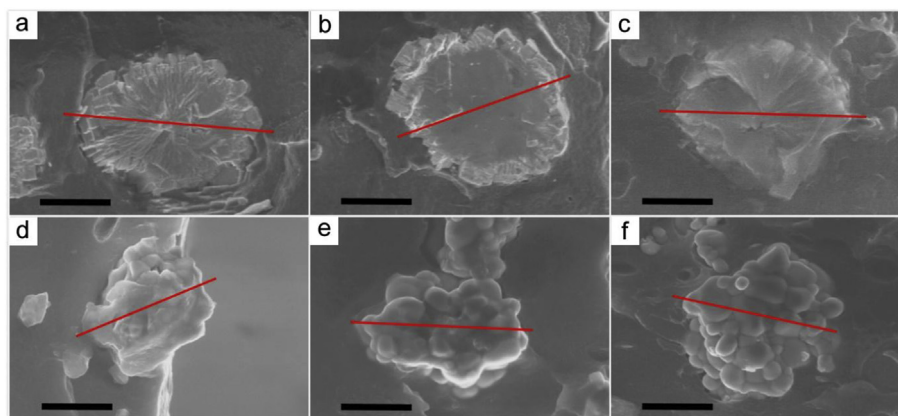

Fig. 3. SEM pictures and EDS line scan positions of the cross section of **(a)** P-12 precursor, **(b)** P-18 precursor, **(c)** P-24 precursor, **(d)** P-12, **(e)** P-18 and **(f)** P-24; the scale bar is 2 μm.
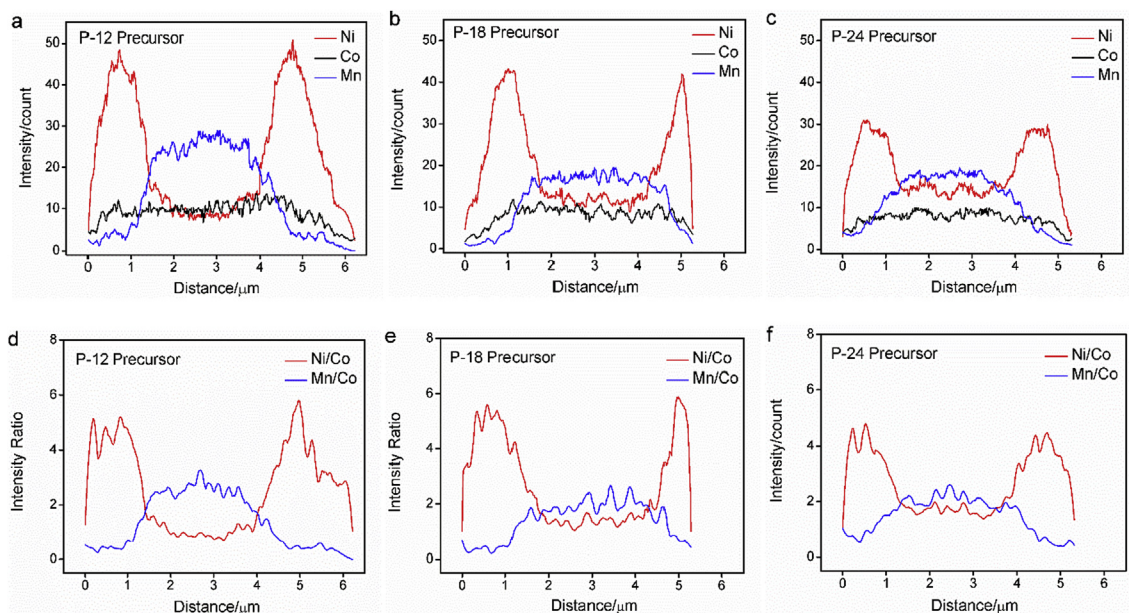
Fig. 4. EDS line scan results of precursors on **(a–c)** transition metal element distribution and **(d–f)** ratios between transition metal elements distribution.
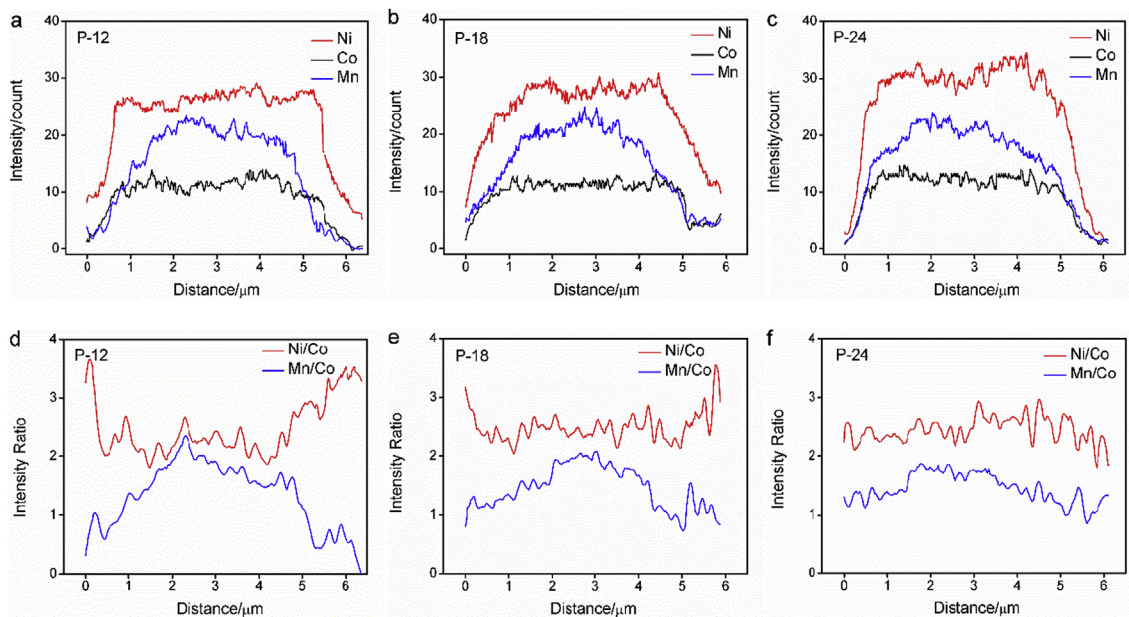

Fig. 5. EDS line scan results of NCM powder on **(a–c)** transition metal element distribution and **(d–f)** ratios between transition metal elements distribution.

voltage, the P-24 samples still show the highest specific capacity and cycling stability. SEM images of the P-12, P-18 and P-24 samples display that their morphology is maintained after cycling in the voltage range of 3–4.6 V (Fig. S2).

The higher Ni content in the outer layer of P-12 powder can lead to a faster capacity decay, because the unstable Ni ions on the particle surface has high reactivity with the electrolyte, therefore resulting in a phase transformation from layered to spinel and rock salt structures [6]. The phase transformation might increase the charge transfer resistance. The outer layer of P-24 powder has relatively low Ni concentration and high Mn concentration, which helps stabilize the near-surface region and limit its reactivity with electrolyte. The uniform transition metal distribution of P-24 powder is an important reason for the best electrochemical performance.

EIS measurements are performed on the cells prepared with P-12, P-18 and P-24 powder to compare the charge transfer resistances of the

three electrodes before cycling and after 50 cycles at discharged state. Fig. 7a shows the Nyquist plots of the cells prepared with P-12, P-18 and P-24 powder after 50 cycles, as well as the corresponding equivalent circuit to fit the plots. R_s is the electrolyte resistance, R_{sei} and R_{ct} demonstrate the resistances of the solid electrolyte interface (SEI) and the charge transfer resistance, respectively. W is the Warburg impedance related to the diffusion of Li$^+$ [37]. The R_{ct} values for P-12, P-18 and P-24 are 58.1, 52.0 and 45.9 Ω, respectively. It turns out that P-24 powder indeed has the lowest R_{ct} value, which correlates well with its relatively lower Ni concentration in the outer layer. This explains its better rate capability than P-12 and P-18. The linear part of EIS in the low frequency is related to Li$^+$ diffusion in electrode and the diffusion coefficient (D) is calculated using the following equation [38]:

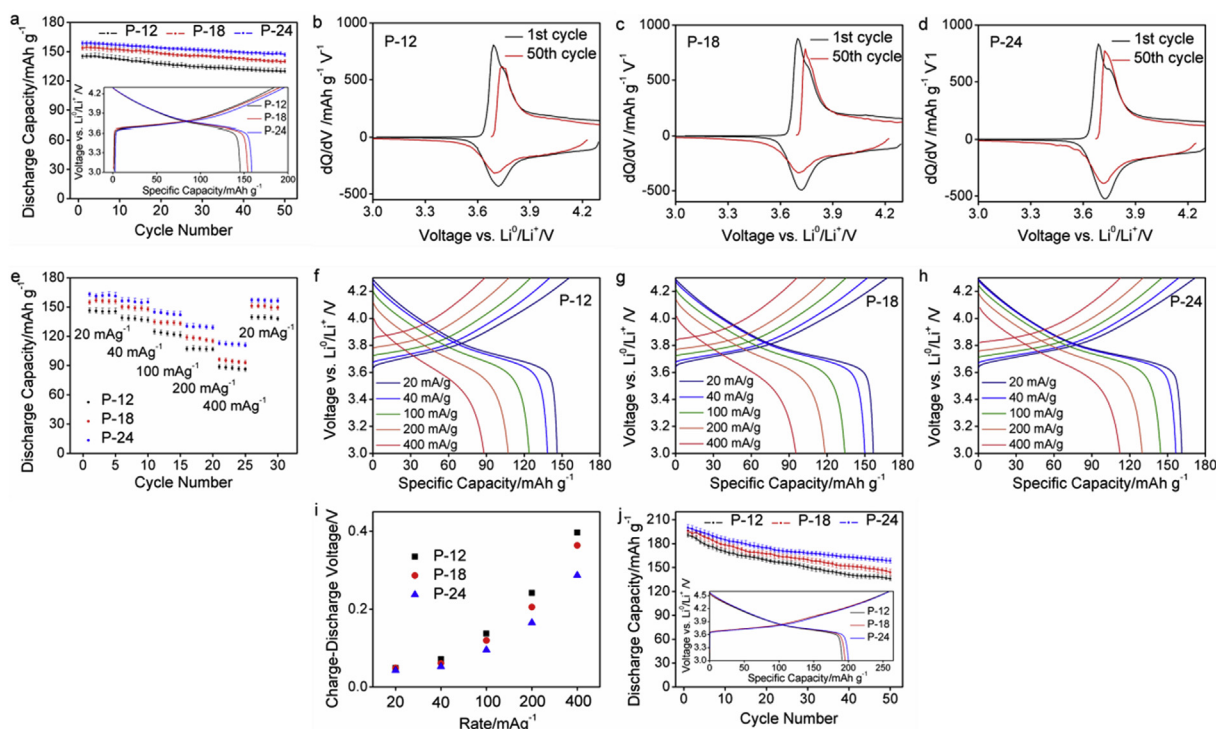$$D = \frac{R^2 T^2}{2A^2 n^4 F^4 C^2 \sigma^2}$$

(2)

Fig. 6. (a) Cycling performance of NCM523 powder in the voltage range of 3–4.3 V at 20 mA g^{-1}, and the error bars show the variation of three cells; the inset shows the first charge-discharge curves. The dQ/dV plots of **(b)** P-12, **(c)** P-18 and **(d)** P-24 samples. **(e)** Rate capabilities of NCM523 powder, and the error bars show the variation of three cells. Charge-discharge curves under different C rate for **(f)** P-12, **(g)** P-18, and **(h)** P-24 samples. **(i)** Voltage differences at the beginning of discharge and charge cycle under different C-rates. **(j)** Cycling performance in the voltage range of 3–4.6 V at 20 mA g^{-1}, and the error bars show the variation of three cells; the inset shows the first charge-discharge curve.
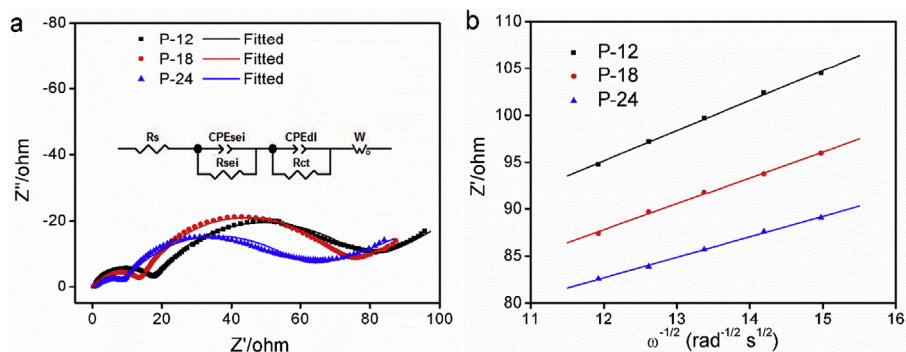

Fig. 7. (a) Nyquist plots, fitting plots and equivalent circuit of P-12, P-18 and P-24 electrodes after 50 cycles. **(b)** Relationship between real parts of the complex impedance and $\omega^{-1/2}$.

R is the gas constant, T is the absolute temperature, A is the interface between cathode and electrolyte ($A = 1.6\ cm^2$), n is the number of electrons involved in reaction (n = 1), F is the Faraday constant, C is the concentration of Li$^+$ in the electrode ($= \rho/M$) based on the molecular weight of NCM523 (M) and density (ρ), and σ is the Warburg factor. The Warburg factor can be obtained from the slope of Z′ vs. $\omega^{-1/2}$ plots (ω is the angular frequency) in the Warburg region. The results of the Z′ vs. $\omega^{-1/2}$ and the linear fitting curves are shown in Fig. 7b. The Li$^+$ diffusion coefficients for P-12, P-18 and P-24 are 2.45×10^{-10}, 3.26×10^{-10} and $5.28 \times 10^{-10}\ cm^2\ s^{-1}$, respectively. The highest D for P-24 electrode indicates that its crystal structure facilitates the diffusion of Li$^+$ after an extended time of hydrothermal treatment, which further explains its best rate capability. The highest D values for P-24 can be ascribed to its lowest degree of Li/Ni cation mixing (Table 2). Li/Ni cation mixing can deteriorate the electrochemical performance of the cathode material because it blocks the Li$^+$ transportation channel [39]. It was reported previously that a hydrothermal treatment could decrease the cation mixing of NCM cathode [22]. Even though the reason for this decrease is still not clear, it is speculated that high temperature and pressure environment might provide the energy for regular arrangement of atoms in their own sites, considering Li/Ni cation mixing is a thermodynamically favorable process. The exact mechanism is an important topic of our future study.

The provide extra evidence for the effect of Ni and Mn distribution on the oxidation state of Ni and Mn ions in cathodes after cycling, XPS measurement was performed on cycled P-12, P-18 and P-24 cathodes (Fig. 8). The Ni 2p spectrum has two dominant peaks at 855.5 eV (2p$_{3/2}$) and 873.5 eV (2p$_{1/3}$) which represent Ni^{2+} [40]. The two less dominant shake-up peaks at 860.0 eV and 879.0 eV further confirm the existence of Ni^{2+} [41]. However, less prominent peaks at 857.3, 863.8, 876.9 and 882.1 eV indicate the existence of Ni^{3+} [41]. The Mn 2p spectrum has two major peaks at 645.3 eV (2p$_{3/2}$) and 657.1 (2p$_{1/3}$) which represent Mn^{4+}, with little satellite structure observed [40]. However, less prominent peaks at 646.9 and 658.2 eV indicate the
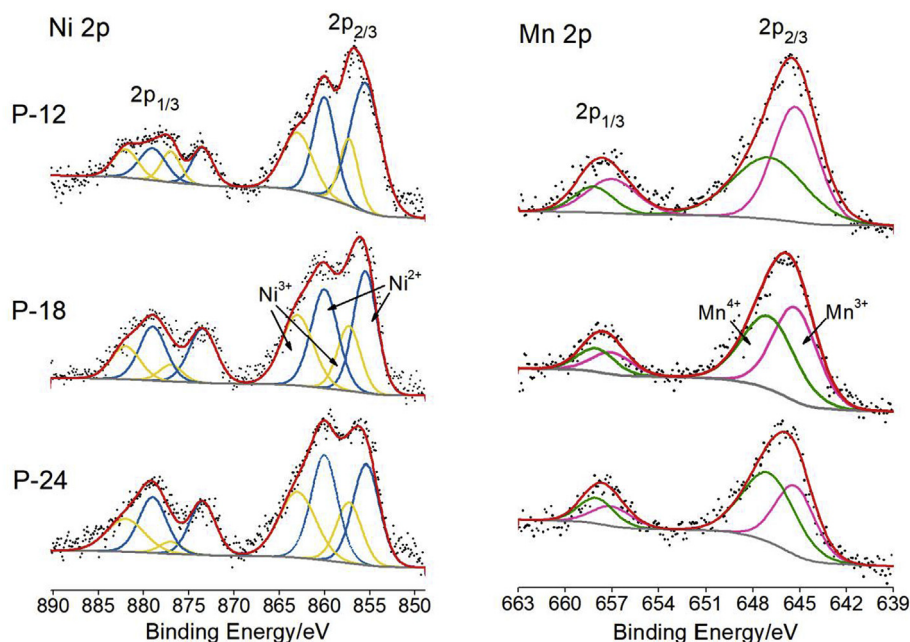
Fig. 8. XPS patterns of P-12, P-18 and P-24 cathodes after 50 cycles.

Table 3
Atomic concentration of Ni and Mn ions in XPS measurement.

Sample	Ni^{2+}/%	Ni^{3+}/%	Mn^{3+}/%	Mn^{4+}/%
P-12	64.56	35.44	55.57	44.43
P-18	62.43	37.57	48.70	51.30
P-24	60.54	39.46	43.56	56.44

existence of Mn^{3+} [42]. The atomic concentrations of Ni^{2+}, Ni^{3+}, Mn^{3+}, Mn^{4+} in P-12, P-18 and P-24 cycled cathodes are displayed in Table 3. It is found that P-12 cathode has the highest amount of Ni^{2+} and Mn^{3+}, while P-24 cathode has the lowest amount of Ni^{2+} and Mn^{3+}. The Ni^{2+} concentration at the surface of P-24 cathode has the closest value to the theoretical values of 60% in NCM523 electrode before cycling, which indicates its minimum structural change after cycling. As discussed previously, the higher Ni content in the outer layer of P-12 cathode has higher reactivity with the electrolyte, therefore resulting in an easier phase transformation from layered to spinel and rock salt structures. The layered to spinel transformation suffers from oxygen loss, and results in the formation of Mn^{3+} for charge compensation [43], which explains the higher Mn^{3+} concentration at the surface of P-12 cathode after cycling. The Jahn-Teller distortion of Mn^{3+} can induce stresses and strains, and decrease the electronic conductivity in the cathode [44,45]. In addition, Mn^{3+} disproportionates partially into Mn^{2+} and Mn^{4+}, and some of the Mn^{2+} is dissolved in the electrolyte, which may also plate on the anode and hinder further cycling [46–48]. Cycled P-24 cathode has a Ni^{2+} concentration closest to the theoretical value before cycling, and it has the lowest concentration of Mn^{3+}, both of which explain the better electrochemical performance of P-24 cathode than P-12 and P-18 cathodes.

4. Conclusions

NCM523 cathode material is synthesized through a urea-based hydrothermal method. Three batches of NCM523 powder are compared in morphology, crystal structure and electrochemical performance. The material with a reaction time of 24 h during precursor synthesis delivers the highest discharge capacity of 161.7 mAh g^{-1} in the voltage range of 3–4.3 V. With the increase in reaction time during the precursor

synthesis, the cycling stability and rate capability are both improved. The improvement is attributed to the enhanced Li^+ diffusion coefficient and reduced charge transfer resistance, which result from the low degree of cation mixing and uniform distribution of transition metal ions. This urea-based hydrothermal approach can be applied for the synthesis of NCM series as well as other layer-structured cathode materials for Li-ion battery.

Appendix A. Supplementary data

Supplementary data related to this article can be found at http://dx.doi.org/10.1016/j.jpowsour.2018.05.030.

References

[1] T. Horiba, T. Maeshima, T. Matsumura, M. Koseki, J. Arai, Y. Muranaka, Applications of high power density lithium ion batteries, J. Power Sources 146 (2005) 107.
[2] V. Etacheri, R. Marom, R. Elazari, G. Salitra, D. Aurbach, Challenges in the development of advanced Li-ion batteries: a review, Energy Environ. Sci. 4 (2011) 3243.
[3] M.M. Thackeray, C. Wolverton, E.D. Isaacs, Electrical energy storage for transportation-approaching the limits of, and going beyond, lithium-ion batteries, Energy Environ. Sci. 5 (2012) 7854.
[4] Y. Shi, M. Zhang, D. Qian, Y.S. Meng, Ultrathin Al_2O_3 coatings for improved cycling performance and thermal stability of $LiNi_{0.5}Co_{0.2}Mn_{0.3}O_2$ cathode material, Electrochim. Acta 203 (2016) 154.
[5] M.D. Radin, S. Hy, M. Sina, C. Fang, H. Liu, J. Vinckeviciute, M. Zhang, M.S. Whittingham, Y.S. Meng, A. Van der Ven, Narrowing the gap between theoretical and practical capacities in Li-ion layered oxide cathode materials, Adv. Energy Mater 7 (2017) 1602888.

[6] S.K. Jung, H. Gwon, J. Hong, K.Y. Park, D.H. Seo, H. Kim, J. Hyun, W. Yang, K. Kang, Understanding the degradation mechanisms of LiNi$_{0.5}$Co$_{0.2}$Mn$_{0.3}$O$_2$ cathode material in lithium ion batteries, Adv. Energy Mater 4 (2014) 1300787.

[7] M. Noh, J. Cho, Optimized synthetic conditions of LiNi$_{0.5}$Co$_{0.2}$Mn$_{0.3}$O$_2$ cathode materials for high rate lithium batteries via co-precipitation method, J. Electrochem. Soc. 160 (2013) A105.

[8] J. Zhang, X. Guo, S. Yao, W. Zhu, X. Qiu, Tailored synthesis of Ni$_{0.25}$Mn$_{0.75}$CO$_3$ spherical precursors for high capacity Li-rich cathode materials via a urea-based precipitation method, J. Power Sources 238 (2013) 245.

[9] K.S. Lee, S.T. Myung, J.S. Moon, Y.K. Sun, Particle size effect of Li[Ni$_{0.5}$Mn$_{0.5}$]O$_2$ prepared by co-precipitation, Electrochim. Acta 53 (2008) 6033.

[10] Y.K. Sun, S.T. Myung, B.C. Park, J. Prakash, I. Belharouak, K. Amine, High-energy cathode material for long-life and safe lithium batteries, Nat. Mater. 8 (2009) 320.

[11] R. Zhao, Z. Yang, J. Liang, D. Lu, C. Liang, X. Guan, A. Gao, H. Chen, Understanding the role of Na-doping on Ni-rich layered oxide LiNi$_{0.5}$Co$_{0.2}$Mn$_{0.3}$O$_2$, J. Alloy. Comp. 689 (2016) 318.

[12] Z. Zhang, S. Zhu, J. Huang, C. Yan, Acacia gum-assisted co-precipitating synthesis of LiNi$_{0.5}$Co$_{0.2}$Mn$_{0.3}$O$_2$ cathode material for lithium ion batteries, Ionics 22 (2016) 621.

[13] J.Z. Kong, H.F. Zhai, C. Ren, M.Y. Gao, X. Zhang, H. Li, J.X. Li, Z. Tang, F. Zhou, Synthesis and electrochemical performance of macroporous LiNi$_{0.5}$Co$_{0.2}$Mn$_{0.3}$O$_2$ by a modified sol–gel method, J. Alloy. Comp. 577 (2013) 507.

[14] F. Zhou, X. Zhao, A. van Bommel, A.W. Rowe, J.R. Dahn, Coprecipitation synthesis of Ni$_x$Mn$_{1-x}$(OH)$_2$ mixed hydroxides, Chem. Mater. 22 (2010) 1015.

[15] D. Wang, I. Belharouak, G.M. Koenig, G. Zhou, K. Amine, Growth mechanism of Ni$_{0.3}$Mn$_{0.7}$CO$_3$ precursor for high capacity Li-ion battery cathodes, J. Mater. Chem. 21 (2011) 9290.

[16] J. Fan, G. Li, D. Luo, C. Fu, Q. Li, J. Zheng, L. Li, Hydrothermal-assisted synthesis of Li-rich layered oxide microspheres with high capacity and superior rate-capability as a cathode for lithium-ion batteries, Electrochim. Acta 173 (2015) 7.

[17] F. Wu, M. Wang, Y. Su, L. Bao, S. Chen, A novel method for synthesis of layered LiNi$_{1/3}$Mn$_{1/3}$Co$_{1/3}$O$_2$ as cathode material for lithium-ion battery, J. Power Sources 195 (2010) 2362.

[18] Y. Li, Q. Han, X. Ming, M. Ren, L. Li, W. Ye, X. Zhang, H. Xu, L. Li, Synthesis and characterization of LiNi$_{0.5}$Co$_{0.2}$Mn$_{0.3}$O$_2$ cathode material prepared by a novel hydrothermal process, Ceram. Int. 40 (2014) 14933.

[19] S.T. Myung, M.H. Lee, S. Komaba, N. Kumagai, Y.K. Sun, Hydrothermal synthesis of layered Li[Ni$_{1/3}$Co$_{1/3}$Mn$_{1/3}$]O$_2$ as positive electrode material for lithium secondary battery, Electrochim. Acta 50 (2005) 4800.

[20] J. Xie, X. Huang, Z. Zhu, J. Dai, Hydrothermal synthesis of Li(Ni$_{1/3}$Co$_{1/3}$Mn$_{1/3}$)O$_2$ for lithium rechargeable batteries, Ceram. Int. 36 (2010) 2485.

[21] X. Li, W. He, L. Chen, W. Guo, J. Chen, Z. Xiao, Hydrothermal synthesis and electrochemical performance studies of Al$_2$O$_3$-coated LiNi$_{1/3}$Co$_{1/3}$Mn$_{1/3}$O$_2$ for lithium-ion batteries, Ionics 20 (2014) 833.

[22] W. He, X. Li, J. Chen, F. Peng, R. Zhang, Y. Liu, Z. Xiao, Effects of ionothermal and hydrothermal methods on structure and electrochemical performance of LiNi$_{1/3}$Co$_{1/3}$Mn$_{1/3}$O$_2$ cathode materials, Mater. Chem. Phys. 155 (2015) 9.

[23] S. Komaba, S.T. Myung, N. Kumagai, T. Kanouchi, K. Oikawa, T. Kamiyama, Hydrothermal synthesis of high crystalline orthorhombic LiMnO$_2$ as a cathode material for Li-ion batteries, Solid State Ionics 152 (2002) 311.

[24] W.H. Ryu, S.J. Lim, W.K. Kim, H. Kwon, 3-D dumbbell-like LiNi$_{1/3}$Mn$_{1/3}$Co$_{1/3}$O$_2$ cathode materials assembled with nano-building blocks for lithium-ion batteries, J. Power Sources 257 (2014) 186.

[25] R. Sathiyamoorthi, R. Chandrasekaran, P. Santhosh, K. Saminathan, R. Gangadharan, T. Vasudevan, Electrochemical characterization of nanocrystalline LiM$_x$Co$_{1-x}$O$_2$ (M = Mg, Ca) prepared by a solid-state thermal method, Synth. React. Inorg. Met. Org. Chem. 36 (2006) 71.

[26] K. Yang, J. Su, L. Zhang, Y. Long, X. Lv, Y. Wen, Urea combustion synthesis of LiNi$_{0.5}$Mn$_{1.5}$O$_4$ as a cathode material for lithium ion batteries, Particuology 10 (2012) 765.

[27] O. Sha, S. Wang, Z. Qiao, W. Yuan, Z. Tang, Q. Xu, Y. Su, Synthesis of spinel LiNi$_{0.5}$Mn$_{1.5}$O$_4$ cathode material with excellent cycle stability using urea-based sol–gel method, Mater. Lett. 89 (2012) 251.

[28] T. Risthaus, J. Wang, A. Friesen, R. Krafft, M. Kolek, J. Li, Synthesis of LiNi$_{0.5}$Mn$_{1.5}$O$_4$ cathode materials with different additives: effects on structural, morphological and electrochemical properties, J. Electrochem. Soc. 163 (2016) A2103.

[29] D.Z. He, Q.X. Guo, Q. Yin, J.T. Li, Z.L. Gong, Sol-gel combustion synthesis of Li$_{1.2}$Mn$_{0.54}$Ni$_{0.13}$Co$_{0.13}$O$_2$ as cathode materials for lithium ion batteries, Int. J. Electrochem. Sci. 12 (2017) 455.

[30] L. Su, C. Ma, T. Hou, W. Han, Selective synthesis and capacitive characteristics of CoNiAl three-component layered double hydroxide platelets, RSC Adv. 3 (2013) 19807.

[31] W.H.R. Shaw, J.J. Bordeaux, The decomposition of urea in aqueous media, J. Am. Chem. Soc. 77 (1955) 4729.

[32] P.B. Kelter, M.D. Mosher, A. Scott, Chemistry: the Practical Science, Cengage Learning, 2008.

[33] A. van Bommel, J.R. Dahn, Analysis of the growth mechanism of coprecipitated spherical and dense nickel, manganese, and cobalt-containing hydroxides in the presence of aqueous ammonia, Chem. Mater. 21 (2009) 1500.

[34] K. Ben-Kamel, N. Amdouni, A. Mauger, C.M. Julien, Study of the local structure of LiNi$_{0.33+\delta}$Mn$_{0.33+\delta}$Co$_{0.33-2\delta}$O$_2$ (0.025 ≤ δ ≤ 0.075) oxides, J. Alloy. Comp. 528 (2012) 91.

[35] X. Zhang, A. Mauger, Q. Lu, H. Groult, L. Perrigaud, F. Gendron, C.M. Julien, Synthesis and characterization of LiNi$_{1/3}$Mn$_{1/3}$Co$_{1/3}$O$_2$ by wet-chemical method, Electrochim. Acta 55 (2010) 6440.

[36] P.Y. Hou, L.Q. Zhang, X.P. Gao, A high-energy, full concentration-gradient cathode material with excellent cycle and thermal stability for lithium ion batteries, J. Mater. Chem. A 2 (2014) 17130.

[37] W. Hua, J. Zhang, Z. Zheng, W. Liu, X. Peng, X.D. Guo, B. Zhong, Y.J. Wang, X. Wang, Na-doped Ni-rich LiNi$_{0.5}$Co$_{0.2}$Mn$_{0.3}$O$_2$ cathode material with both high rate capability and high tap density for lithium ion batteries, Dalton Trans. 43 (2014) 14824.

[38] J. Ni, H. Zhou, J. Chen, X. Zhang, Improved electrochemical performance of layered LiNi$_{0.4}$Co$_{0.2}$Mn$_{0.4}$O$_2$ via Li$_2$ZrO$_3$ coating, Electrochim. Acta 53 (2008) 3075.

[39] B.S. Liu, Z.B. Wang, F.D. Yu, Y. Xue, G.J. Wang, Y. Zhang, Y.X. Zhou, Facile strategy of NCA cation mixing regulation and its effect on electrochemical performance, RSC Adv. 6 (2016) 108558.

[40] J. Li, S. Xiong, Y. Liu, Z. Ju, Y. Qian, Uniform LiNi$_{1/3}$Co$_{1/3}$Mn$_{1/3}$O$_2$ hollow microspheres: designed synthesis, topotactical structural transformation and their enhanced electrochemical performance, Nanomater. Energy 2 (2013) 1249.

[41] Z. Chen, J. Wang, D. Chao, T. Baikie, L. Bai, S. Chen, Y. Zhao, T.C. Sum, J. Lin, Z. Shen, Hierarchical porous LiNi$_{1/3}$Co$_{1/3}$Mn$_{1/3}$O$_2$ nano/micro spherical cathode material: minimized cation mixing and improved Li$^+$ mobility for enhanced electrochemical performance, Sci. Rep. 6 (2016) 25771.

[42] B.J. Tan, K.J. Klabunde, P.M.A. Sherwood, XPS studies of solvated metal atom dispersed catalysis-evidence for layered cobalt manganese particles on alumina silica, J. Am. Chem. Soc. 113 (1991) 855.

[43] L. Ben, H. Yu, B. Chen, Y. Chen, Y. Gong, X. Yang, L. Gu, X. Huang, Unusual spinel-to-layered transformation in LiMn$_2$O$_4$ cathode dxplained by electrochemical and thermal stability investigation, ACS Appl. Mater. Interfaces 9 (2017) 35463.

[44] M.E. Arroyo, y de Dompablo, C. Marianetti, A. Van der Ven, G. Ceder, Jahn-Teller mediated ordering in Li$_x$MO$_2$ compounds, Phys. Rev. B 63 (2001) 144107.

[45] C.A. Marianetti, D. Morgan, G. Ceder, First-principles investigation of the cooperative Jahn-Teller effect for octahedrally coordinated transition-metal ions, Phys. Rev. B 63 (2001) 224304.

[46] C.S. Johnson, N.C. Li, C. Lefief, J.T. Vaughey, M.M. Thackeray, Synthesis, characterization and electrochemistry of lithium battery electrodes: xLi2MnO3·(1-x) LiMn0.333Ni0.333Co0.333O2 (0 < = x < = 0.7), Chem. Mater. 20 (2008) 6095.

[47] M.N. Ates, Q. Jia, A. Shah, A. Busnaina, S. Mukerjee, K.M. Abraham, Mitigation of layered to spinel conversion of a Li-rich layered metal oxide cathode material for Li-ion batteries, J. Electrochem. Soc. 161 (2014) A290.

[48] R. Hausbrand, G. Cherkashinin, H. Ehrenberg, M. Gröting, K. Albe, C. Hess, W. Jaegermann, Fundamental degradation mechanisms of layered oxide Li-ion battery cathode materials: methodology, insights and novel approaches, Mater. Sci. Eng. B 192 (2015) 3.